Plutonium in Southern Yellow Sea sediments and its implications for the quantification of oceanic-derived mercury and zinc☆

Jinlong Wang [b, d], Jinzhou Du [a], Jian Zheng [b], Qianqian Bi [a], Yu Ke [c], Jianguo Qu [a, *]

[a] State Key Laboratory of Estuarine and Coastal Research, East China Normal University, Shanghai, 200241, PR China
[b] Center for Advanced Radiation Emergency Medicine, National Institutes for Quantum and Radiological Science and Technology, 4-9-1 Anagawa, Inage, Chiba, 263-8555, Japan
[c] East China Sea Environmental Monitoring Center, State Oceanic Administration, Shanghai, 201206, PR China
[d] Biospheric Assessment for Waste Disposal Team, National Institute of Radiological Sciences, National Institutes for Quantum and Radiological Science and Technology, 4-9-1 Anagawa, Inage, Chiba, 263-8555, Japan

ARTICLE INFO

ABSTRACT

The spatial distributions of mercury (Hg) and zinc (Zn) concentration and the isotopic composition of plutonium (Pu) were investigated in surface sediments and sediment cores collected from the Southern Yellow Sea (SYS) during May 2014. The variation of the ^{240}Pu/^{239}Pu atom ratio (0.18−0.31) in the surface sediments of the SYS clearly indicated a signal of close-in fallout input from the Pacific Proving Ground (PPG). The buried $^{239+240}$Pu in the sediment of the SYS was estimated to be $(4.7 \pm 0.5) \times 10^{10}$ Bq y^{-1} during the period from 2011 to 2014, of which ~33% $(1.5 \times 10^{10}$ Bq y$^{-1})$ was derived from the PPG by long-range transport via ocean currents (e.g., the North Equatorial Current and Kuroshio Current). The concentrations of Hg and Zn varied from 0.003 to 0.067 mg kg^{-1} and from 43.9 to 137 mg kg^{-1}, respectively, and exhibited positive correlations with the $^{239+240}$Pu activity both in the surface sediments (0−1 cm) and upper layers (7 cm) of the sediment cores. Therefore, by using Pu as a tracer, we estimated that the oceanic input contributed 2.0 tons y^{-1} of Hg and 1.0×10^{3} tons y^{-1} of Zn to the SYS sediments between 2011 and 2014, which accounted for 33% and 3% of total buried Hg and Zn, respectively. These findings indicate that environmental pollution control should also consider the oceanic contribution of some pollutants. The results of the present work help to elucidate the biogeochemical cycling of trace metals in marginal seas, and are helpful for managing environmental pollution in marine environments.

© 2020 Elsevier Ltd. All rights reserved.

1. Introduction

Marginal seas are key areas for strong land-ocean interactions, and can be highly active and important sinks for radionuclides (e.g., plutonium (Pu)), organic pollutants (e.g., PCBs)/inorganic pollutants (heavy metals) and biogenic elements. These pollutants and elements can be affected by physical, chemical, and biological processes, which co-occur and interact (Aller et al., 2010; McKee et al., 2004; Santos et al., 2008). Due to the accumulation of heavy metals, the surface sediments in a marginal sea system could be toxic to sediment-dwelling organisms and fish, and considerable attention has focused on assessing the distribution patterns and sources of heavy metals (Yuan et al., 2012). To assess and manage

heavy metals pollution, it is essential to undertaken a quantitative source discrimination. Traditionally, the main sources of heavy metals have been considered to be atmospheric fallout and riverine input (e. g., Amos et al., 2014; Corbitt et al., 2011; Radakovitch et al., 2008). Considering the very high volumes of oceanic currents that can be transported from the open ocean to marginal seas (e.g., Kuroshio Current (KC)) (Zhai et al., 2014), a certain amount of the heavy metals that are deposited into the open ocean via the atmosphere can be transported to marginal seas via currents. Moreover, mercury (Hg) is highly toxic and volatile and can be transported over longer distances via the atmosphere in comparison to other metals (e.g., zinc (Zn)), and it is supposed that the oceanic input flux of Hg differs to that of other metals.

In the Northwest Pacific (NP), massive nuclear tests were performed in the Pacific Proving Grounds (PPG) during the 1950s, which resulted in a 5.1 PBq of local (troposphere) fallout of Pu with a ^{240}Pu/^{239}Pu atom ratio of 0.33−0.36 (Buesseler, 1997; Hamilton,

2005). Using this distinct ratio with global fallout (0.18, Kelley et al., 1999) as a tracer, studies have suggested that Pu derived from the PPG can be transported to marginal seas (e.g., the East China Sea (ECS)) of the NP and even to the Indian Ocean via the North Equatorial Current (NEC) and other relevant currents (Hao et al., 2018; Liu et al., 2011; Pittauer et al., 2017; Wang et al., 2017; Zheng and Yamada, 2004, 2006). In the area surrounding the Southern Yellow Sea (SYS), the $^{240}Pu/^{239}Pu$ atom ratio (~0.18) in the sediments of the north Jiangsu tidal flats (Liu et al., 2013) and those in the seawater around the Korean Peninsula (0.18−0.30; Kim et al., 2004) indicate that the hypothesis of the transport of Pu derived from the PPG- in the NP marginal seas deserves further examination.

The Yellow Sea (YS) is a semi-enclosed shallow sea in the NP marginal sea system. Biogenic elements and pollutants in the SYS have diverse sources due to anthropogenic factors (e.g., industrial and domestic wastewater) and a complex current system (Fig. 1). The Changjiang Diluted Water (CDW) and other small rivers (i.e., the Daguhe, Huaihe, Han, Keum, Mankyong and Yeongsan) discharge freshwater into the SYS. The Yellow Sea Warm Current (YSWC) is a branch of the KC and also transports a massive volume of warm and salty water to the SYS. Due to the influences of anthropogenic and natural factors, the SYS suffers from increasing environmental issues, such as eutrophication, as well as a certain level of heavy metal pollution (Liu et al., 2017; Xu et al., 2018). The sedimentary deposition of pollutants, trace elements and nutrients has also attracted considerable attention due to the complex current system and multiple potential sources. These include sediment discharge from the modern Yellow River, Changjiang and other small rivers, as well as erosion from the old Yellow River delta near the Subei shoal (Bian et al., 2013; Park et al., 2000; Wang et al., 2016). These geological and hydrological settings make the SYS an ideal region for investigating land-ocean interactions and the 'source' to 'sink' of pollutants, trace elements, and nutrients. Studies have reported the distribution and ecological risk assessment of heavy metals (e.g., Hg and Zn) in the sediments of the SYS and have

emphasized the important role of atmospheric deposition as a source of metals (He et al., 2009; Liu et al., 2016b; Xu et al., 2018; Yuan et al., 2012). However, the estimation of the oceanic input of metals to the SYS is still lacking, which limits the strength of environmental protection policy in this region.

Although studies have reported the distribution of Pu in marginal sea systems, (see Wang et al. (2017) for a summary), the spatial distribution patterns of ^{239}Pu and ^{240}Pu concentration, as well as their atomic compositions in the sediments of the SYS, are still unknown. Moreover, a quantitative estimation of the oceanic input of heavy metals to the SYS is lacking. Therefore, this study aims to determine the $^{239+240}Pu$ concentration and $^{240}Pu/^{239}Pu$ atom ratio in the surface sediments of the SYS and to investigate oceanic Pu and heavy metals (Zn and Hg) in the SYS. As mentioned above, the oceanic flux of volatile Hg is expected to differ to that of Zn; thus, Hg and Zn (as a comparable element) are selected in this work to estimate their oceanic input fluxes. This study will help to elucidate the transport and fate of oceanic Pu and other particle-reactive species including heavy metals in the SYS.

2. Materials and methods

During a research cruise on R/V "Dongfanghong 2" in May 2014, 39 surface sediments (0−1 cm) and 2 sediment cores (Fig. 1) were collected. The sediment cores (core No. 21: 23 cm in length; core No. 34: 19 cm in length) were subsampled from sediments collected in a box core using 10-cm diameter Plexiglas core tubes. Then each sediment core was sliced into 1-cm thick layers before being stored at 4 °C awaiting laboratory analysis (Wang et al., 2016). Details of sampling locations, sampling dates, and water depths at each station are listed in the Supporting Information (Table S1).

The method used to analyze the concentrations of Hg and Zn in the surface sediment samples was similar to that of Zhang et al. (2009). Briefly, approximately 250 mg of each dried sediment sample was digested in a mixture of 10 mL of HNO_3, 5.0 mL of $HClO_4$ and 5.0 mL of HF. After the solid residue disappeared, the digested
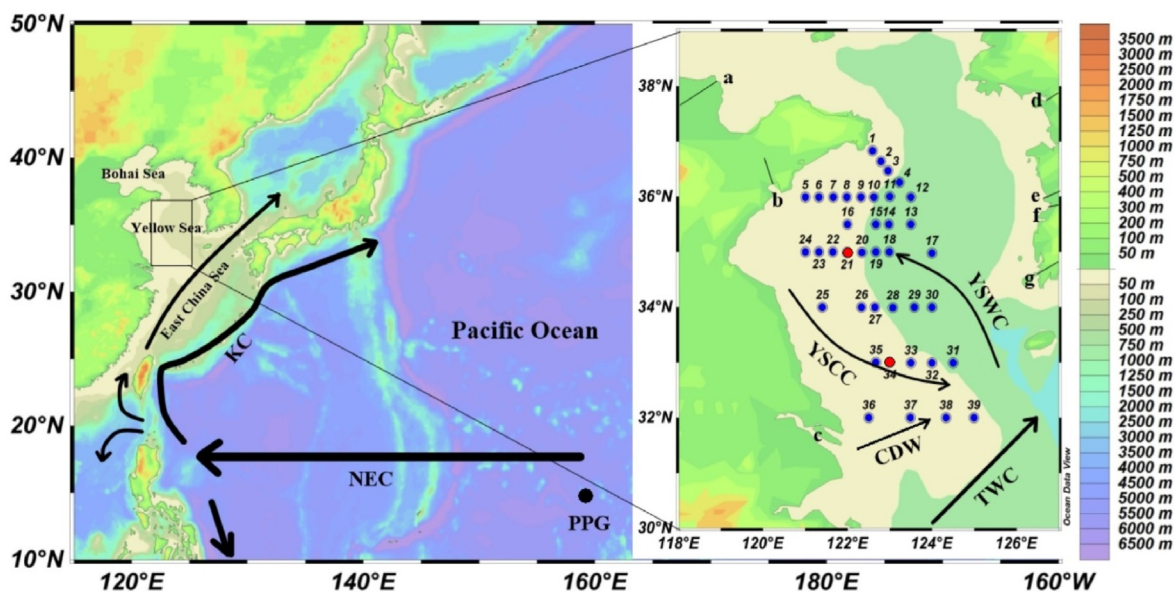

Fig. 1. Sampling location in the Southern Yellow Sea. The current system of the SYS is described as in Wu et al. (2018) and Hu et al. (2015): Changjiang Diluted Water (CDW), Yellow Sea Coastal Current (YSCC), Yellow Sea Warm Current (YSWC), Taiwan Warm Current (TWC), Kuroshio Current (KC), and North Equatorial Current (NEC). The red and blue dots represent the sampling locations of the sediment cores and surface sediments, respectively. Several rivers are also plotted, including a: Yellow River, b: Daguhe, c: Changjiang, d: Han River, e: Keum River, f: Mankyong River, g: Yeongsan River. (For interpretation of the references to colour in this figure legend, the reader is referred to the Web version of this article.)

solutions were used to measure Zn and Hg using graphite furnace atomic absorption spectrometry (Perkin Elmer AAnalyst 800) and atomic fluorescence spectrometry (PF6), respectively (further details are provided in Supporting Information).

The separation method for Pu was modified from Ketterer et al. (2002). Briefly, 3 g of each dried sediment sample was ashed, spiked with 1 mBq ^{242}Pu (NISTSRM- 4334/g), separated and purified using TEVA resin (100−150 μm). The Pu was measured using high-resolution inductively coupled plasma mass spectrometry (HR-ICP-MS) (Element II, Thermo Fisher Scientific, Waltham, MA), equipped with a desolvation sample introduction system (Aridus II, CETAC, USA) (More details were shown in Supporting Information, Lindahl et al., 2010).

3. Results and discussion

3.1. Spatial distribution of Pu isotopes in the surface sediments of the SYS

The grain size, $^{239+240}$Pu activity, and ^{240}Pu/^{239}Pu atom ratio data for the surface sediments are listed in Table S1. The $^{239+240}$Pu activity varied widely as the values ranging from 0.014 to 0.659 Bq kg^{-1} (mean of 0.186 ± 0.142 Bq kg^{-1}, whereby the reported error is the standard deviation of 39 data points, geometric mean: 0.133 Bq kg^{-1}). The maximum values of $^{239+240}$Pu were observed in the northeast part of the SYS, and values above the mean were also found in the southeast part of the SYS (Fig. 2). The regions with higher values of $^{239+240}$Pu might be related to the lower sedimentation rate (0.1−0.3 cm y^{-1}) relative to that in the western region (0.2−0.5 cm y^{-1}) of the SYS (Qiao et al., 2017) and to the finer grain size of surface sediments (4−10 μm) (Table S1). Generally, finer surface sediments with more sorption sites had a higher $^{239+240}$Pu activity. However, the correlation between the $^{239+240}$Pu concentration and grain size was notably weak (r = −0.22, p = 0.17). This suggests that the distribution of the $^{239+240}$Pu activity was also affected by many other factors, for example, the mineral component of sediments, organic matter content, sources of $^{239+240}$Pu, and hydrological and geomorphological conditions (Baskaran et al., 1996; Laceby et al., 2017). In the southeast part of the SYS, multiple currents (i.e., the CDW, TWC, YSCC and YSWC) intersect, and a counterclockwise circulation exists (Naimie et al., 2001). Such strong hydrodynamic conditions might reinforce particle resuspension and later enhance the scavenging of Pu from the water column to the surface sediments (Crusius et al., 2004).

The ^{240}Pu/^{239}Pu atom ratio of surface sediments in the SYS ranged from 0.176 to 0.308 (arithmetic mean: 0.226 ± 0.033, geometric mean: 0.224), which is in the range of the global fallout value (0.18) (Kelley et al., 1999) and the PPG signal (0.33−0.36) (Buesseler, 1997). The ^{240}Pu/^{239}Pu atom ratio in Chinese and Japanese soil profiles was reported to be ~0.18, which is distinctly different to that of the Semipalatinsk and Lop Nur nuclear tests (<0.1) as well as the Chernobyl and Fukushima accidents (>0.32)
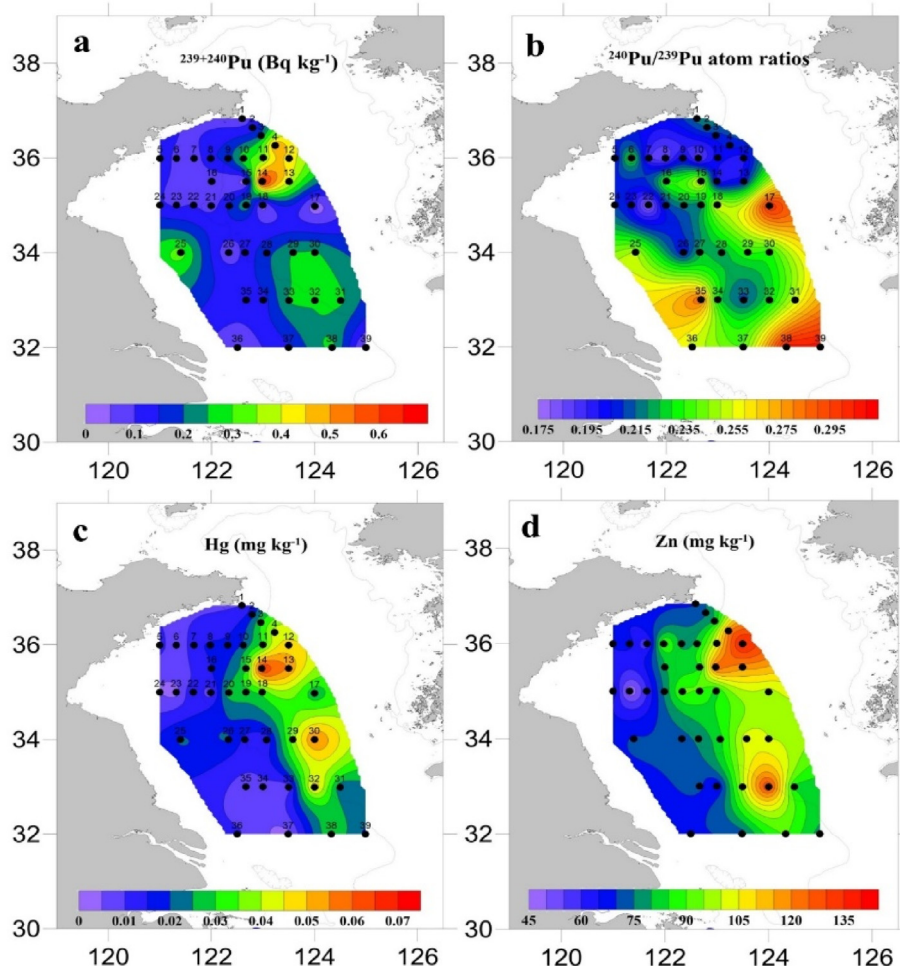

Fig. 2. Spatial distribution of $^{239+240}$Pu activity (a), ^{240}Pu/^{239}Pu atom ratio values (b), Hg (c) and Zn (d) concentrations (mg kg^{-1}) in the surface sediments of the SYS in May 2014.

(Boulyga et al., 1997; Muramatsu et al., 2003; Zheng et al., 2009; Zheng et al., 2012; Bu et al., 2014, 2015). This suggests that the close-in fallout from these incidents was negligible for the Chinese shore region associated with the SYS. For the emissions from nuclear power reactors on the coasts of the SYS, the $^{240}Pu/^{239}Pu$ atom ratio was reported to be ~0.18 in the sediments of the north Jiangsu tidal flats, which indicates that these contributions were negligible (Liu et al., 2013; Liu et al., 2016a). Therefore, higher ratios should be attributed to the transport of Pu from the PPG via the NEC, KC and YSWC. Relatively low ratios (i.e., 0.18−0.21) were distributed in the regions corresponding to the flow pathway of the YSCC (Zhu and Wu, 2018). Due to the fact that the YSWC is intermittent, with a salinity that is indistinguishable relative to that of the YSCC, the specific flow direction cannot be obtained by physical oceanography observations (Wu et al., 2018). However, the $^{240}Pu/^{239}Pu$ atom ratio distribution indicated a clear flow direction of the YSCC, which is expected to help characterize the current system in this region. Higher ratios in the southwest part of the SYS might be due to the carryover effect of the TWC (Wu et al., 2018).

3.2. Spatial distribution of Hg and Zn in the surface sediments of the SYS

The concentrations of Hg and Zn varied from 0.003 to 0.067 mg kg^{-1} (mean: 0.017 ± 0.016 mg kg^{-1}) and from 43.9 to 137.3 mg kg^{-1} (mean: 82.5 ± 20.7 mg kg^{-1}), respectively (Fig. 2). Higher concentrations of Hg and Zn were observed in the central part of the SYS and decreased towards the coast. This might be related to the fine grain size and high concentration of total organic carbon (TOC) in the central region (Xing et al., 2011) because these factors may lead to an increased absorption of trace metals (Swarzenski et al., 2006). However, the correlations between grain size and the Hg concentration (r = −0.33, p = 0.04) and Zn concentration (r = −0.41, p = 0.01) were very weak. A previous study reported that the Hg concentration of surface sediments in the SYS had a positive correlation (r = 0.61, p < 0.01) with the TOC concentration, whereas Zn was poorly correlated with the TOC concentration (r = 0.41, p = 0.02) (Yuan et al., 2012). These findings suggest that multiple factors affect the distribution of heavy metal, and include sedimentation rates, mineral components, and current systems (Swarzenski et al., 2006). Expectedly, the Hg and Zn concentrations showed similar distribution patterns to that of the $^{239+240}Pu$ activity. The positively linear correlation (Fig. 3) between the $^{239+240}Pu$ activity and Hg concentration (r = 0.70, p < 0.01) and Zn concentration (r = 0.69, p < 0.01) indicates that both particle-

reactive metals and Pu are scavenged to approximately the same degree (Ravichandran et al., 1995; Wang and Yamada, 2005).

3.3. Temporal variations of Pu, Zn and Hg in the sediment cores from the SYS

The grain size, $^{239+240}Pu$ activity, $^{240}Pu/^{239}Pu$ atom ratio, Hg concentration and Zn concentration data for the two sediment cores are listed in Table S2. The maximum Pu layer corresponding to 1963 varied due to changes in the sedimentation rate. By assuming that sedimentary deposition was relatively stable over the past six decades and that the $^{239+240}Pu$ depositional flux did not change, Pu can be used to date recent sediments. From Fig. 4, the maximum $^{239+240}Pu$ activity corresponding to 1963 was found at a depth of 12−13 cm for core 21 and 14−15 cm for 34. Then the linear sedimentation rates were calculated to be 0.25 ± 0.02 and 0.28 ± 0.02 cm y^{-1} for core 21 and 34 after considering the uncertainty (1.0 cm) from the resolution of sub-sectioning. These values were very close to the linear sedimentation rate based on the Constant Initial Concentration (CIC) model of $^{210}Pb_{ex}$ (0.23 ± 0.03 cm y^{-1} for core 21 and 0.29 ± 0.07 cm y^{-1} for core 34). Using the Constant Rate of Supply (CRS) model of $^{210}Pb_{ex}$, the vertical profile of the age of the two sediment cores was obtained (Fig. 4). It can be seen that the CIC and $^{239+240}Pu$ activity based on the sediment age agreed well, and that the three model-based sediment ages also agreed well in the upper 14 cm of the two sediment cores. Below a depth of 14 cm, the CRS model age became significantly older and less reliable than that of the CIC and the $^{239+240}Pu$ (Fig. 4). The CRS model relies on $^{210}Pb_{ex}$ inventories. This model-based ages are sensitive to changes in $^{210}Pb_{ex}$ accumulation, sediment focusing, and erosion. The trapping efficiency of ^{210}Pb and an overestimation of age by the CRS model in comparison to the CIC model are common, especially in the deeper layers of sediment cores (Appleby, 2008; Jweda and Baskaran, 2011; Baskaran et al., 2015). The penetration of $^{239+240}Pu$ corresponding to the sediment age of each sediment core reached levels older than 1952, which should be related to the post depositional migration of $^{239+240}Pu$. Such a migration broadens the global fallout peak without shifting the peak (Baskaran et al., 2017). The $^{240}Pu/^{239}Pu$ atom ratio in each sediment core was >0.18 and nearly uniform with depth. The higher values recorded in the sediment profiles suggest a continuous contribution from the local Pu-fallout of the PPG. The irregular distribution of the $^{240}Pu/^{239}Pu$ atom ratio should be related to the pre-depositional mixing process, which can also be evidenced by the broad peak of $^{239+240}Pu$ activity.

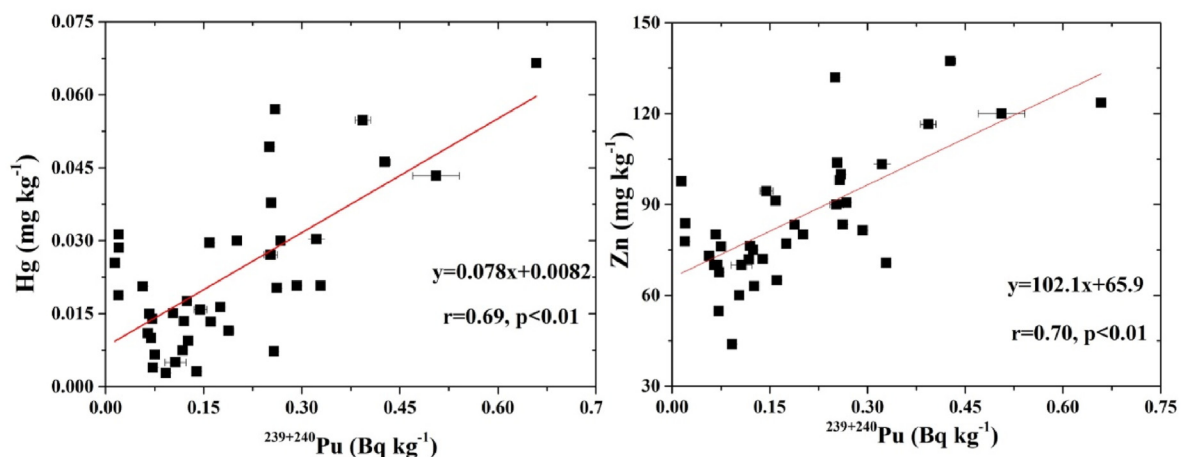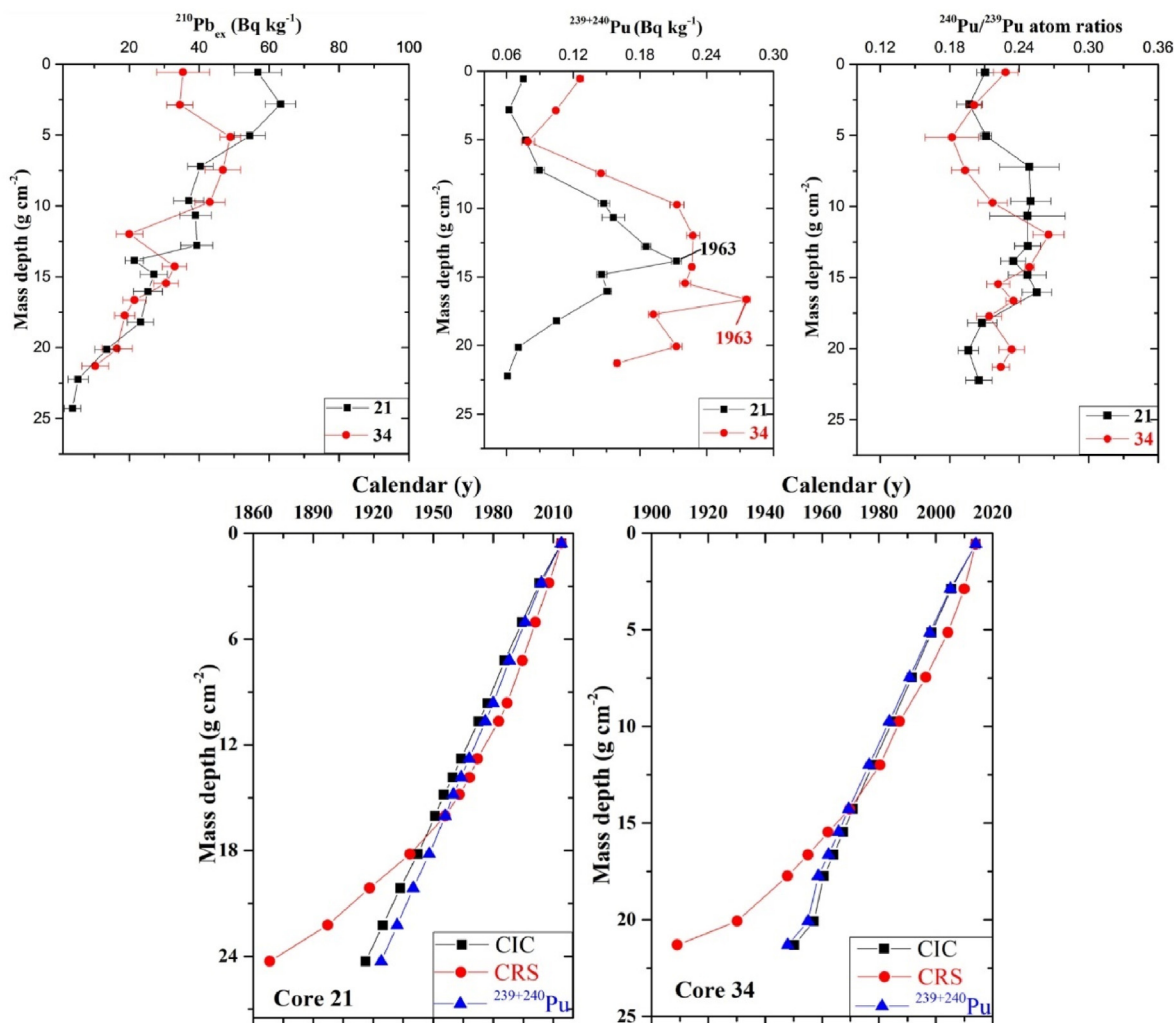**Fig. 3.** Linear correlation between the $^{239+240}Pu$ activity and Hg and Zn concentrations.

Fig. 4. Vertical profiles of $^{210}Pb_{ex}$, $^{239+240}Pu$, $^{240}Pu/^{239}Pu$ atom ratio, and sediment ages based on three methods.

The inventories of $^{239+240}Pu$ and $^{210}Pb_{ex}$, which were obtained from the integration of their activities in each layer multiplied by the mass depth of that layer, were 26 ± 2.2 Bq m^{-2} and 8.3 ± 1.0 kBq m^{-2} for core 21, respectively, and 38 ± 3 Bq m^{-2} and 6.9 ± 1.1 kBq m^{-2} for core 34, respectively. The atmospheric deposition of $^{239+240}Pu$ (42 Bq m^{-2}) between 30°N and 40°N was higher than the calculated $^{239+240}Pu$ inventory in both cores of the SYS. For the atmospheric deposition of $^{210}Pb_{ex}$, although there are no reported data, other data from the nearest stations at the same latitude as the SYS (i.e., Qingdao to the north (36.1°N) and Shanghai to the south (31.20°N)) can be used. The mean annual atmospheric fallout flux of $^{210}Pb_{ex}$ in Qingdao and Shanghai have been reported to be 186 and 366 Bq m^{-2} y^{-1}, respectively (Yi et al., 2005; Du et al., 2010). Then the atmospheric depositional of $^{210}Pb_{ex}$ was calculated to be 8.9 ± 4.1 kBq m^{-2} by using the mean lifetime of ^{210}Pb (32 y) multiplied by the mean annual atmospheric fallout flux of 276 ± 127 Bq m^{-2} y^{-1} in the two cities. This value was higher than the measured $^{210}Pb_{ex}$ inventory in each of the sediment core from the SYS. A higher atmospheric deposition of both $^{239+240}Pu$ and $^{210}Pb_{ex}$ in comparison to the measured sedimentary inventories suggests that i) the sedimentary particles did not significantly recycle in the water column, and ii) there was no sediment focusing causing an accelerated sediment deposition (Swarzenski et al., 2006).

As the sedimentation rates based on the CIC model of $^{210}Pb_{ex}$ and $^{239+240}Pu$ agreed well, we used the sedimentation rate based on $^{239+240}Pu$ activity to reconstruct the temporal variations of the Zn and Hg concentrations in the two sediment cores below (Fig. 5). In core 21, the maximum concentrations of Hg (0.074 mg kg^{-1}) and Zn (82.4 mg kg^{-1}) corresponded to 1980 and 1988, respectively. In sediment core 34, the maximum values of Hg and Zn were found at 1985 and 1992, respectively. These findings are related to some extent to the maximum global metal emissions (e.g., Cu, Pb and Zn) during the 1980s and 1990s (Nriagu, 1996). The positively linear correlations between $^{239+240}Pu$ activity and concentrations of Hg and Zn in the upper 7 cm layer of both sediment cores (core 21: r = 0.98, p = 0.02 for Zn, and r = 0.71, p = 0.28 for Hg; core 34: r = 0.83, p = 0.17 for Zn, and r = 0.75, p = 0.25 for Hg) further suggest that these two metals and Pu were approximately scavenged to the same degree.

3.4. Pollutants transported from the ocean to margin seas

Many studies have addressed the important contribution of atmospheric deposition to the Zn and Hg inputs to marginal seas. The atmospheric fallout of these metals to the open ocean can be transported to marginal seas, where they are subsequently scavenged by suspended particles as the particle concentration is
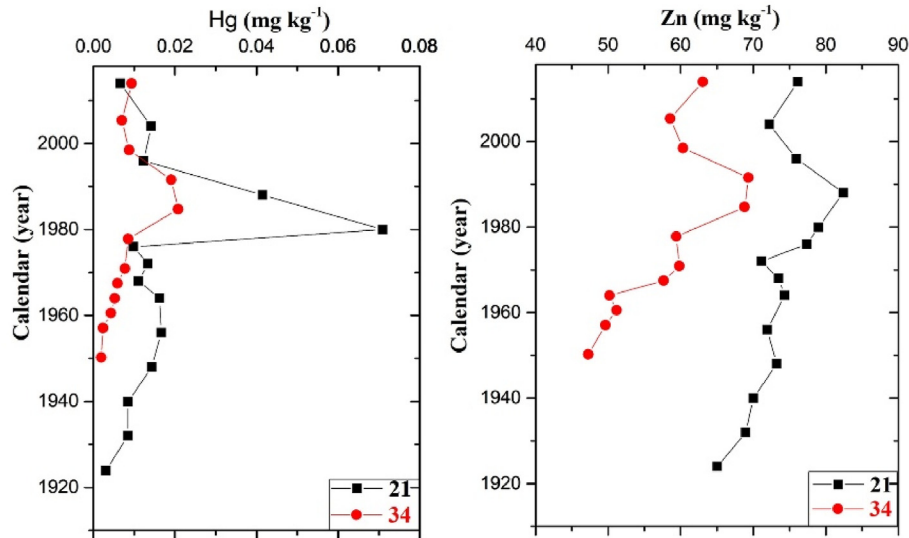
Fig. 5. Temporal variation of Hg and Zn concentrations in two sediment cores collected from the SYS during May 2014.

considerably higher in comparison to the open ocean. As discussed above, the positive correlations between the $^{239+240}$Pu activity and Hg and Zn concentrations in the core profiles allowed us to assume that metals and Pu were approximately scavenged to the same degree. Thus, after estimating the oceanic input of $^{239+240}$Pu, the oceanic input of heavy metals could also be assessed based on the correlation between Pu and metals (Wang et al., 2017). The annually buried $^{239+240}$Pu in the sediments was calculated using equation:

$$B_x = A_x \times \rho \times R \times S \tag{1}$$

where A_x is the geometric mean activity of $^{239+240}$Pu in the surface sediments of the SYS (in the 1 cm layer) (0.133 Bq kg^{-1}, n = 39), ρ is the mean bulk density of the surface sediments (1100 kg m^{-3}), R is the median sedimentation rate in the SYS (0.29 ± 0.03 cm y^{-1}, n = 50, Qiao et al., 2017), and S is the total surface area (1.19 × 10^5 km^2) of the SYS. Thus, we estimated the annually buried $^{239+240}$Pu in the SYS to be (4.7 ± 0.5) × 10^{10} Bq (Fig. 6). Considering the depth of the surface sediments (0−1 cm) and the median sedimentation rate (0.29 ± 0.03 cm y^{-1}) in the SYS, this buried $^{239+240}$Pu value approximately represents a mean value for the period from 2011 to 2014.

The contribution of atmospheric fallout in the SYS in this three year period should have been very small as a result of the cessation of nuclear testing since the late 1970s. The mean atmospheric flux of ^{137}Cs in Shanghai (31.2 °N, 121.4 °E), a city near the SYS, during 2006 and 2007 was reported to be 0.33 Bq m^{-2} y^{-1} (Du et al., 2010), and it can be assumed that the flux in 2014 should have been smaller than this. The global fallout $^{239+240}$Pu/^{137}Cs activity ratio was reported to be 0.021 (UNSCEAR, 2000), and the global fallout $^{239+240}$Pu was calculated to be 6.9 × 10^{-3} Bq m^{-2} y^{-1}. By taking the surface area of the SYS (1.19 × 10^5 km^2), we estimated the atmospheric fallout of $^{239+240}$Pu to be approximately 8.2 × 10^8 Bq y^{-1}, which is <1.0% of buried $^{239+240}$Pu in the SYS and can be considered to be negligible. However, there is a certain amount of riverine input to the SYS. The sediment discharge from the Daguhe and Huaihe in China and the Han, Keum, Mankyong and Yeongsan rivers in Korea into the SYS at an estimated rate of 7.9 × 10^6 ton y^{-1} (Qiao et al., 2017). In addition, the Yellow River and other small rivers also discharge sedimentary particles into the Bohai Sea and the Northern YS, and a small portion of these particles may be transported to the middle (35.5 °N) of the SYS (Yang and Liu, 2007). The ^{240}Pu/^{239}Pu atom ratios in Chinese soils were reported to be 0.18 (Zheng et al., 2009, 2012; Bu et al., 2014, 2015; Xu et al., 2015); thus, the riverine input of the ^{240}Pu/^{239}Pu atom ratio was also assumed to be 0.18. The lower ^{240}Pu/^{239}Pu atom ratio values (~0.18) observed in the northern part of the SYS (e.g., stations 12 and 14)
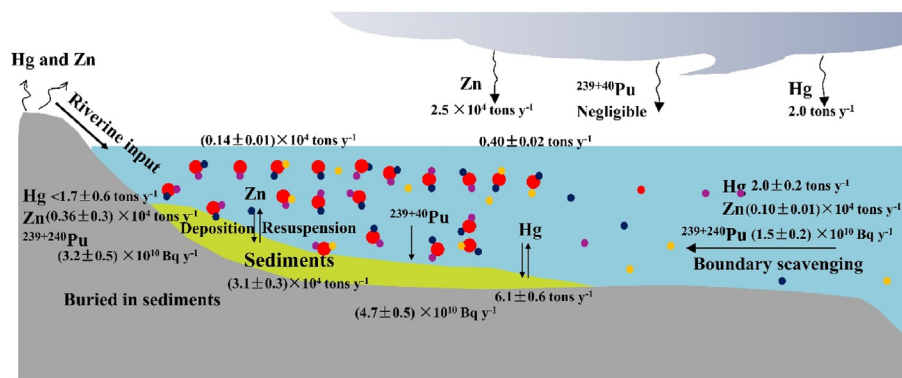

Fig. 6. Cycling of $^{239+240}$Pu Hg and Zn in the sediments of the SYS.

support the hypothesis of particles being transport mainly by the Yellow River. This means that the riverine input and the PPG input serve as two major endmembers of Pu in the SYS, with a $^{240}Pu/^{239}Pu$ atom ratio of 0.18 and 0.33, respectively (Buesseler, 1997). It has been found that Pu binds strongly to sediment particles (Sholkovitz, 1983; Wang et al., 2020), and that Pu desorption from sediments to seawater in the Irish Sea was <1% (Francis et al., 2008); hence the release of Pu from sediments in the SYS can assumed to be negligible. Thus, the relative Pu contribution of the input from the PPG can be estimated by a simple two end-member mixing model (Krey et al., 1976). Using a geometric mean $^{240}Pu/^{239}Pu$ atom ratio of 0.224 in the surface sediment of the SYS, we estimated a Pu contribution from the PPG to sediments of the SYS of 32.6%. Using this value of the buried $^{239+240}Pu$ in the SYS, the PPG input $^{239+240}Pu$ was estimated to be $(1.5 \pm 0.2) \times 10^{10}$ Bq y^{-1}.

The annually buried Hg and Zn can be estimated using Equation (1), in which A_x is expressed as the mean concentrations of Hg (0.017 mg kg^{-1}) and Zn (82.3 mg kg^{-1}), with values of 6.1 ± 0.6 and $(3.1 \pm 0.3) \times 10^4$ tons, respectively. Using the correlation between Pu and these metals (i.e., [Hg] = 0.078[$^{239+240}Pu$]+0.0082 and [Zn] = 102.1[$^{239+240}Pu$]+65.9), we estimated an oceanic input of Hg and Zn is 2.0 ± 0.2 and $(1.0 \pm 0.1) \times 10^3$ tons y^{-1}, respectively. The oceanic input of Hg represents approximately 33% of the SYS buried Hg, whereas that of Zn only accounts for 3% of the buried Zn. This could be related to the fact that Hg can be transported farther than Zn via the atmosphere due to its volatility; thus, considerably more Hg than Zn may be deposited to the open ocean.

Although there are no known direct measurements of the atmospheric deposition of Hg and Zn to the SYS, data from Qingdao station to the west (36.1° N, 120.8 °E) was used as this is the nearest station at a similar latitude to the SYS. Yuan et al. (2012) reported an atmospheric depositional flux of Zn to the SYS of 213 mg m^{-2} y^{-1}, which was based on the measurement in Qingdao. Using this value, we estimated the contribution of Zn from atmospheric deposition to the SYS for a surface area of 1.19×10^5 km^2 to be 2.5×10^4 tons y^{-1}. For Hg, a previous study reported that the atmospheric depositional flux in Qingdao was 0.126 μg m^{-2} day^{-1} on a 'dust day' and 0.04 μg m^{-2} day^{-1} on a 'non-dust day' (Zhang et al., 2015). During 2014, there were 24 days with dust in Qingdao; thus, we obtained an annually depositional Hg flux of 16.7 μg m^{-2} y^{-1}. Subsequently, we estimated the atmospheric deposition Hg to the SYS to be 2.0 tons y^{-1}.

The release of metals from sediment also contributes a fraction of the metals in the SYS. It is hard to directly estimate such a contribution due to the limited number of investigations of the diffusive flux from the sediments of the SYS. Yuan et al (2004) reported that the exchangeable Zn (extracted by acetic acid) accounted for 4.1%–4.7% (mean: 4.5% ± 0.2%) of the total Zn in the sediment of ECS, which is located to the south of the SYS. This fraction of Zn could be potentially released to seawater due to sediment resuspension and mixing. Using this mean value for the ECS, we estimated that sediment release could contribute $(0.14 \pm 0.01) \times 10^4$ ton y^{-1} of Zn to the SYS.

The estimated diffusive flux of monomethylmercury (MMHg) from coastal marine deposits varied both spatially and seasonally and ranged from 9 to 2300 pmol m^{-2} day^{-1} (Fitzgerald et al., 2007). The median of this reported flux, i.e., 46 ± 2 pmol m^{-2} day^{-1}, was used to estimate the diffusive MMHg from the sediment of the SYS, which yielded 0.40 ± 0.02 ton y^{-1}. The total diffusive Hg from sediment of the SYS should be higher than this estimation considering the complex sedimentary redox process (Ma et al., 2018) and the sediment resuspension due to the strong hydrodynamic condition in the SYS (Luo et al., 2017). Consequently, we obtained a riverine input of 1.7 ± 0.6 tons y^{-1} for Hg and $(0.36 \pm 0.30) \times 10^4$ tons y^{-1} for Zn. It should be noted that this

estimation is a lower limit because the Pu mass balance showed that a portion of particles would be transported from the SYS to the ECS. From the mass balance of the two metals (Fig. 6), we found that most of the Zn was sourced from atmospheric deposition (81%), whereas the oceanic input (3%), sediment release (4%) and riverine input (12%) only contributed small fractions. In contrast, atmospheric deposition and oceanic input were the main source of Hg (33% and 33%, respectively), and riverine input (28%) and sediment release (6%) also contributed considerable amounts of Hg.

The suspended particulate matter (SPM) concentration in marginal seas is often higher than that in the open ocean. For example, Ren et al., 2011 found that the SPM concentration in the offshore surface waters of the SYS was approximately 4–10 mg L^{-1}, whereas that of the bottom waters was much higher, with a reported maximum value of >138 mg L^{-1}. The distribution coefficients of Hg and Zn are known to be generally higher in coastal areas in comparison to the open ocean (Nyffeler et al., 1984; Tang et al., 2002). Thus, dissolved and colloidal metals can be scavenged from the water column and deposited to the sediments along with suspended particles, and can be transported from the open ocean into marginal seas via ocean currents (Fig. 6) (Honeyman et al., 1988; Zheng and Yamada, 2006). The use Pu as a tracer could also be potentially used to quantitatively assess the transport of other particle-reactive categories (e.g., inorganic and organic pollutants) from the open ocean to marginal seas.

3.5. Implications for the biogeochemical cycle of trace metals and environmental management

Although a number of studies have addressed the significance of the oceanic input radionuclides to marginal seas, the oceanic contribution of trace metals to marginal sea has not yet attracted sufficient attention (Santschi et al., 1999; Zheng and Yamada, 2006). A previous study reported that riverine inputs were the dominant source of Hg to the marginal seas of the Pacific Ocean (Amos et al., 2014). The authors also noted that their estimation was associated with large uncertainties due to the use of sparse data and a large variability in the Hg concentration in rivers. Our estimation also suggested that riverine inputs represent an important source of Hg to the SYS; however, we also highlighted the importance of oceanic contributions. Accordingly, the oceanic contribution should be considered in the mass balance estimation of Hg in marginal seas, and may prevent the overestimation of riverine contributions. In contrast, although the present estimation indicates that Zn in the SYS was mainly sourced from atmospheric fallout and riverine input (Yuan et al., 2012), the oceanic input of Zn is much smaller than that of Hg. This phenomenon suggests that one explanation for the enhanced Hg and Zn concentrations in the southeast part of the SYS is the efficient scavenging of oceanic trace metals transported via the YSWC and KC. To further clarify the specific sources of trace metals in different regions of the SYS, it would be worth investigation the isotopic compositions in the future (Andersen et al., 2011; Feng et al., 2010). Overall, the results of the present work provide an initial insight into the assessment of trace metal budgets in marginal seas, especial heavy metals such as Hg.

To control environmental pollution in marginal seas, the sources of pollutants should be clearly re-evaluated. Previous studies have reported levels of Hg and Zn pollution in the SYS (Ci et al., 2016; Yuan et al., 2012). To manage Hg pollution in the SYS, controlling only the terrigenous input seems inefficient because of oceanic sources. Although riverine input and atmospheric fallout would be reduced, the oceanic input would be sustained because of the large buffering capacity of the open ocean. As discussed above, the buried Hg would be released into the seawater by sediment resuspension and/or the sedimentary redox process

(Hammerschmidt and Fitzgerald, 2006; Merritt and Amirbahman, 2007). This type of release could also be expected for Zn even if riverine input and atmospheric fallout were to decrease. Thus, the oceanic contribution and the release from benthic sediments should be considered when environmental protection policies are implemented in marginal seas. The results of this study are expected to be helpful for monitoring and controlling environmental pollution in marine environments.

4. Conclusions

The spatial distribution and vertical profiles of Pu, Hg, and Zn were investigated in the SYS. The variation in the ^{240}Pu/^{239}Pu atom ratio (0.18−0.31) in the surface sediment samples and sediment cores from the SYS clearly indicated a signal of the Pu close-in fallout from the PPG. The maximum concentrations of Hg and Zn in the sediment cores corresponded to the 1980s and 1990s, which was the period with the maximum global fallout of heavy metals. The buried $^{239+240}$Pu in the sediments of the SYS was estimated to be $(4.7 \pm 0.5) \times 10^{10}$ Bq y^{-1} for the period from 2011 to 2014, in which ~33% (1.5×10^{10} Bq y^{-1}) was derived from the PPG by long-range transport via ocean currents. The concentrations of Hg and Zn both exhibited positive correlations with $^{239+240}$Pu activity, both in the surface sediments and upper layers of the sediment cores. Using Pu as a tracer, we estimated that the oceanic input contributed 2.0 tons y^{-1} of Hg and 1.0×10^3 tons y^{-1} of Zn to the sediments of the SYS between 2011 and 2014, which accounted for 33% and 3% of the total buried Hg and Zn, respectively. These findings indicate that environmental pollution control should also consider the oceanic contribution of some pollutants. The results of the present work can help to elucidate the biogeochemical cycling of trace metals in marginal seas.

CRediT authorship contribution statement

Jinlong Wang: Conceptualization, Methodology, Funding acquisition, Writing - original draft. **Jinzhou Du:** Conceptualization, Writing - review & editing. **Jian Zheng:** Writing - review & editing, Funding acquisition. **Qianqian Bi:** Methodology. **Yu Ke:** Methodology. **Jianguo Qu:** Methodology, Writing - review & editing.

Declaration of competing interest

The authors declare that they have no known competing financial interests or personal relationships that could have appeared to influence the work reported in this paper.

Appendix A. Supplementary data

Supplementary data to this article can be found online at https://doi.org/10.1016/j.envpol.2020.115262.

References

Aller, R.C., Madrid, V., Chistoserdov, A., Aller, J.Y., Heilbrun, C., 2010. Unsteady diagenetic processes and sulfur biogeochemistry in tropical deltaic muds: implications for oceanic isotope cycles and the sedimentary record. Geochem. Cosmochim. Acta 74 (16), 4671−4692.

Amos, H.M., Jacob, D.J., Kocman, D., Horowitz, H.M., Zhang, Y., Dutkiewicz, S., Horvat, M., Corbitt, M.S., Krabbenhof, D.P., Sunderland, E.M., 2014. Global biogeochemical implications of mercury discharges from rivers and sediment burial. Environ. Sci. Technol. 48 (16), 9514−9522.

Andersen, M.B., Vance, D., Archer, C., Anderson, R.F., Ellwood, M.J., Allen, C.S., 2011. The Zn abundance and isotopic composition of diatom frustules, a proxy for Zn availability in ocean surface seawater. Earth Planet Sci. Lett. 301 (1−2), 137−145.

Appleby, P.G., 2008. Three decades of dating recent sediments by fallout radionuclides: a review. Holocene 18 (1), 83−93.

Baskaran, M., Asbill, S., Santschi, P., Brooks, J., Champ, M., Adkinson, D., Colmer, M.R., Makeyev, V., 1996. Pu, ^{137}Cs and excess ^{210}Pb in Russian Artic sediments. Earth Planet Sci. Lett. 140, 243−257.

Baskaran, M., Miller, C.J., Kumar, A., Andersen, E., Hui, J., Selegean, J.P., Creech, C.T., Barkach, J., 2015. Sediment accumulation rates and sediment dynamics using five different methods in a well-constrained impoundment: case study from Union Lake, Michigan. J. Great Lake. Res. 41 (2), 607−617.

Baskaran, M., Bianchi, T.S., Filley, T.R., 2017. Inconsistencies between ^{14}C and short-lived radionuclides-based sediment accumulation rates: effects of long-term remineralization. J. Environ. Radioact. 174, 10−16.

Bian, C., Jiang, W., Greatbatch, R.J., 2013. An exploratory model study of sediment transport sources and deposits in the Bohai Sea, Yellow Sea, and East China Sea. J. Geophys. Res. Oceans 118 (11), 5908−5923.

Boulyga, S.F., Erdmann, N., Funk, H., Kievets, M.K., Lomonosova, E.M., Mansel, A., Trautmann, N., Yaroshevich, O.I., Zhuk, I.V., 1997. Determination of isotopic composition of plutonium in hot particles of the Chernobyl area. Radiat. Meas. 28 (1−6), 349−352.

Bu, W., Zheng, J., Guo, Q.J., Uchida, S., 2014. Vertical distribution and migration of global fallout Pu in forest soils in southwestern China. J. Environ. Radioact. 136, 174−180.

Bu, W., Ni, Y., Guo, Q., Zheng, J., Uchida, S., 2015. Pu isotopes in soils collected downwind from Lop Nor: regional fallout vs. global fallout. Sci. Rep. 5, 12262. https://doi.org/10.1038/srep12262.

Buesseler, K.O., 1997. The isotopic signature of fallout plutonium in the North Pacific. J. Environ. Radioact. 36 (1), 69−83.

Ci, Z., Zhang, X., Yin, Y., Chen, J., Wang, S., 2016. Mercury redox chemistry in waters of the eastern Asian seas: from polluted coast to clean open ocean. Environ. Sci. Technol. 50 (5), 2371−2380.

Corbitt, E.S., Jacob, D.J., Holmes, C.D., Streets, D.G., Sunderland, E.M., 2011. Global source−receptor relationships for mercury deposition under present-day and 2050 emissions scenarios. Environ. Sci. Technol. 45 (24), 10477−10484.

Crusius, J., Bothner, M.H., Sommerfield, C.K., 2004. Bioturbation depths, rates and processes in Massachusetts Bay sediments inferred from modeling of ^{210}Pb and $^{239+240}$Pu profiles. Estuar. Coast. Shelf Sci. 61, 643−655.

Du, J., Wu, Y., Huang, D., Zhang, J., 2010. Use of ^{7}Be, ^{210}Pb and ^{137}Cs tracers to the transport of surface sediments of the Changjiang Estuary, China. J. Mar. Syst. 82 (4), 286−294.

Feng, X., Foucher, D., Hintelmann, H., Yan, H., He, T., Qiu, G., 2010. Tracing mercury contamination sources in sediments using mercury isotope compositions. Environ. Sci. Technol. 44 (9), 3363−3368.

Fitzgerald, W.F., Lamborg, C.H., Hammerschmidt, C.R., 2007. Marine biogeochemical cycling of mercury. Chem. Rev. 107 (2), 641−662.

Francis, A.J., Dodge, C.J., Gillow, J.B., 2008. Reductive dissolution of Pu (IV) by Clostridium sp. under anaerobic conditions. Environ. Sci. Technol. 42 (7), 2355−2360.

Hamilton, T.F., 2005. Linking legacies of the cold war to arrival of anthropogenic radionuclides in the oceans through the 20th century. Radioact. Environ. 6, 23−78.

Hammerschmidt, C.R., Fitzgerald, W.F., 2006. Methylmercury cycling in sediments on the continental shelf of southern New England. Geochem. Cosmochim. Acta 70 (4), 918−930.

Hao, Y., Xu, Y., Pan, S., Song, X., Zhang, K., Guo, H., Gu, Z., 2018. Sources of plutonium isotopes and ^{137}Cs in coastal seawaters of Liaodong Bay and Bohai Strait, China and its environmental implications. Mar. Pollut. Bull. 130, 240−248.

He, Z., Song, J., Zhang, N., Zhang, P., Xu, Y., 2009. Variation characteristics and ecological risk of heavy metals in the south Yellow Sea surface sediments. Environ. Monit. Assess. 157 (1−4), 515−528.

Honeyman, B.D., Balistrieri, L.S., Murray, J.W., 1988. Oceanic trace metal scavenging: the importance of particle concentration. Deep Sea Res. Part I. 35 (2), 227−246.

Hu, D., Wu, L., Cai, W., Gupta, A.S., Ganachaud, A., Qiu, B., Gordon, A.L., Lin, X., Chen, Z., Hu, S., Wang, G., Wang, Q., Sprintall, J., Qu, T., Kashino, Y., Wang, F., Kessler, W., 2015. Pacific western boundary currents and their roles in climate. Nature 522 (7556), 299−308.

Jweda, J., Baskaran, M., 2011. Interconnected riverine−lacustrine systems as sedimentary repositories: case study in southeast Michigan using ^{210}Pb and ^{137}Cs-based sediment accumulation and mixing models. J. Great Lake. Res. 37 (3), 432−446.

Kelley, J.M., Bond, L.A., Beasley, T.M., 1999. Global distribution of Pu isotopes and ^{237}Np. Sci. Total Environ. 237/238, 483−500.

Ketterer, M.E., Watson, B.R., Matisoff, G., Wilson, C.G., 2002. Rapid dating of recent aquatic sediments using Pu activities and ^{240}Pu/^{239}Pu as determined by quadrupole inductively coupled plasma mass spectrometry. Environ. Sci. Technol. 36 (6), 1307–1311.

Kim, C.K., Kim, C.S., Chang, B.U., Choi, S.W., Chung, C.S., Hong, G.H., Hirose, H., Igarashi, Y., 2004. Plutonium isotopes in seas around the Korean Peninsula. Sci. Total Environ. 318, 197–209.

Krey, P.W., Hardy, E.P., Pachucki, C., Rourke, F., Coluzza, J., Benson, W.K., 1976. Massisotopic composition of global fallout plutonium in soil. In: Transuranium Nuclides in the Environment (Proceedings Series). IAEA, Vienna, pp. 671–678.

Laceby, J.P., Evrard, O., Smith, H.G., Blake, W.H., Olley, J.M., Minella, J.P., Owens, P.N., 2017. The challenges and opportunities of addressing particle size effects in sediment source fingerprinting: a review. Earth-Sci. Revs. 169, 85–103.

Lindahl, P., Keith-Roach, M., Worsfold, P., Choi, M.S., Shin, H.S., Lee, S.H., 2010. Ultra-trace determination of plutonium in marine samples using multi-collector inductively coupled plasma mass spectrometry. Anal. Chim. Acta 671 (1–2), 61–69.

Liu, D., Hou, X., Du, J., Zhang, L., Zhou, W., 2016a. ^{129}I and its species in the East China Sea: level, distribution, sources and tracing water masses exchange and movement. Sci. Rep. 6, 36611. https://doi.org/10.1038/srep36611.

Liu, J.A., Su, N., Wang, X., Du, J., 2017. Submarine groundwater discharge and associated nutrient fluxes into the Southern Yellow Sea: a case study for semi-enclosed and oligotrophic seas-implication for green tide bloom. J. Geophys. Res. Oceans 122 (1), 139–152.

Liu, M., Chen, L., Wang, X., Zhang, W., Tong, Y., Ou, L., Xie, H., Shen, H., Ye, X., Deng, C., Wang, H., 2016b. Mercury export from mainland China to adjacent seas and its influence on the marine mercury balance. Environ. Sci. Technol. 50 (12), 6224–6232.

Liu, Z.Y., Zheng, J., Pan, S.M., Gao, J.H., 2013. Anthropogenic plutonium in the north Jiangsu tidal flats of the Yellow Sea in China. Environ. Monit. Assess. 185, 6539–6551.

Liu, Z.Y., Zheng, J., Pan, S., Dong, W., Yamada, M., Aono, T., Guo, Q., 2011. Pu and ^{137}Cs in the Yangtze River Estuary sediments: distribution and source identification. Environ. Sci. Technol. 45 (5), 1805–1811.

Luo, Z., Zhu, J., Wu, H., Li, X., 2017. Dynamics of the sediment plume over the Yangtze bank in the Yellow and East China seas. J. Geophys. Res. Oceans 122 (12), 10073–10090.

Ma, W.W., Zhu, M.X., Yang, G.P., Li, T., 2018. Iron geochemistry and organic carbon preservation by iron (oxyhydr) oxides in surface sediments of the East China Sea and the south Yellow Sea. J. Mar. Syst. 178, 62–74.

McKee, B.A., Aller, R.C., Allison, M.A., Bianchi, T.S., Kineke, G.C., 2004. Transport and transformation of dissolved and particulate materials on continental margins influenced by major rivers: benthic boundary layer and seabed processes. Continent. Shelf Res. 24 (7–8), 899–926.

Merritt, K.A., Amirbahman, A., 2007. Mercury mobilization in estuarine sediment porewaters: a diffusive gel time-series study. Environ. Sci. Technol. 41 (3), 717–722.

Muramatsu, Y., Yoshida, S., Tanaka, A., 2003. Determination of Pu concentration and its isotope ratio in Japanese soils by HR-ICP-MS. J. Radioanal. Nucl. Chem. 255 (3), 477–480.

Naimie, C.E., Blain, C.A., Lynch, D.R., 2001. Seasonal mean circulation in the Yellow Sea-a model-generated climatology. Continent. Shelf Res. 21 (6–7), 667–695.

Nriagu, J.O., 1996. A history of global metal pollution. Science 272 (5259), 223-223.

Nyffeler, U.P., Li, Y.H., Santschi, P.H., 1984. A kinetic approach to describe trace-element distribution between particles and solution in natural aquatic systems. Geochem. Cosmochim. Acta 48 (7), 1513–1522.

Park, S.C., Lee, H.H., Han, H.S., Lee, G.H., Kim, D.C., Yoo, D.G., 2000. Evolution of late Quaternary mud deposits and recent sediment budget in the southeastern Yellow Sea. Mar. Geol. 170 (3–4), 271–288.

Pittauer, D., Tims, S.G., Froehlich, M.B., Fifield, L.K., Wallner, A., McNeil, S.D., Fischer, H.W., 2017. Continuous transport of Pacific-derived anthropogenic radionuclides towards the Indian Ocean. Sci. Rep. 7, 44679. https://doi.org/10.1038/srep44679.

Qiao, S., Shi, X., Wang, G., Zhou, L., Hu, B., Hu, L., Yang, G., Liu, Y., Yao, Z., Liu, S., 2017. Sediment accumulation and budget in the Bohai Sea, Yellow Sea and East China sea. Mar. Geol. 390, 270–281.

Radakovitch, O., Roussiez, V., Ollivier, P., Ludwig, W., Grenz, C., Probst, J.L., 2008. Input of particulate heavy metals from rivers and associated sedimentary deposits on the Gulf of Lion continental shelf. Estuar. Coast Shelf Sci. 77 (2), 285–295.

Ravichandran, M., Baskaran, M., Santschi, P.H., Bianchi, T.S., 1995. Geochronology of sediments in the Sabine-Neches estuary, Texas, USA. Chem. Geol. 125, 291–306.

Ren, J.L., Zhang, G.L., Zhang, J., Shi, J.H., Liu, S.M., Li, F.M., Jin, J., Liu, C.G., 2011.

Distribution of dissolved aluminum in the Southern Yellow Sea: influences of a dust storm and the spring bloom. Mar. Chem. 125 (1–4), 69–81.

Santos, I.R., Burnett, W.C., Godoy, J.M., 2008. Radionuclides as tracers of coastal processes in Brazil: review, synthesis, and perspectives. Braz. J. Oceanogr. 56 (2), 115–130.

Santschi, P.H., Guo, L., Walsh, I.D., Quigley, M.S., Baskaran, M., 1999. Boundary exchange and scavenging of radionuclides in continental margin waters of the Middle Atlantic Bight: implications for organic carbon fluxes. Continent. Shelf Res. 19 (5), 609–636.

Sholkovitz, E.R., 1983. The geochemistry of plutonium in fresh and marine water environments. Earth Sci. Rev. 19 (2), 95–161.

Swarzenski, P.W., Baskaran, M., Rosenbauer, R.J., Orem, W.H., 2006. Historical trace element distribution in sediments from the Mississippi River delta. Estuar. Coast 29 (6), 1094–1107.

Tang, D., Warnken, K.W., Santschi, P.H., 2002. Distribution and partitioning of trace metals (Cd, Cu, Ni, Pb, Zn) in Galveston bay waters. Mar. Chem. 78 (1), 29–45.

UNSCEAR, 2000. United Nations Scientific Committee on the Effects of Atomic Radiation Exposures to the Public from Man-Made Sources of Radiation, Sources and Effects of Ionizing Radiation. United Nations, New York, p. 654.

Wang, J., Du, J., Baskaran, M., Zhang, J., 2016. Mobile mud dynamics in the East China Sea elucidated using ^{210}Pb, ^{137}Cs, ^{7}Be, and ^{234}Th as tracers. J. Geophys. Res. Oceans 121 (1), 224–239.

Wang, J., Baskaran, M., Hou, X., Du, J., Zhang, J., 2017. Historical changes in ^{239}Pu and ^{240}Pu sources in sedimentary records in the East China Sea: implications for provenance and transportation. Earth Planet Sci. Lett. 466, 32–42.

Wang, J., Du, J., Zheng, J., 2020. Plutonium isotopes research in the marine environment: a synthesis. J. Nucl. Radiochem. Sci. 20, 1–11.

Wang, Z.L., Yamada, M., 2005. Plutonium activities and ^{240}Pu/^{239}Pu atom ratios in sediment cores from the East China Sea and Okinawa Trough: sources and inventories. Earth Planet Sci. Lett. 233, 441–453.

Wu, H., Gu, J., Zhu, P., 2018. Winter counter-wind transport in the inner southwestern Yellow Sea. J. Geophys. Res. Oceans 123, 411–436.

Xu, F., Hu, B., Yuan, S., Zhao, Y., Dou, Y., Jiang, Z., Yin, X., 2018. Heavy metals in surface sediments of the continental shelf of the South Yellow Sea and East China Sea: sources, distribution and contamination. Catena 160, 194–200.

Xing, L., Tao, S., Zhang, H., Liu, Y., Yu, Z., Zhao, M., 2011. Distributions and origins of lipid biomarkers in surface sediments from the southern Yellow Sea. Appl. Geochem. 26 (8), 1584–1593.

Xu, Y., Qiao, J., Pan, S., Hou, X., Roos, P., Cao, L., 2015. Plutonium as a tracer for soil erosion assessment in northeast China. Sci. Total Environ. 511, 176–185.

Yang, Z.S., Liu, J.P., 2007. A unique Yellow River-derived distal subaqueous delta in the Yellow Sea. Mar. Geol. 240 (1–4), 169–176, 240(1-4).

Yi, Y., Bai, J., Liu, G., Yang, W., Yi, Q., Huang, Y., Chen, H., 2005. Measurements of atmospheric depositional fluxes of ^{7}Be, ^{210}Pb and ^{210}Po [in Chinese with English abstract]. Mar. Sci. 29 (12), 20–24.

Yuan, H., Song, J., Li, X., Li, N., Duan, L., 2012. Distribution and contamination of heavy metals in surface sediments of the South Yellow Sea. Mar. Pollut. Bull. 64 (10), 2151–2159, 64(10).

Zhai, F., Wang, Q., Wang, F., Hu, D., 2014. Variation of the north equatorial current, mindanao current, and Kuroshio current in a high-resolution data assimilation during 2008–2012. Adv. Atmos. Sci. 31 (6), 1445–1459.

Zhang, W., Feng, H., Chang, J., Qu, J., Xie, H., Yu, L., 2009. Heavy metal contamination in surface sediments of Yangtze River intertidal zone: an assessment from different indexes. Environ. Pollut. 157 (5), 1533–1543.

Zhang, Y., Liu, R., Wang, Y., Cui, X., Qi, J., 2015. Change characteristic of atmospheric particulate mercury during dust weather of spring in Qingdao, China. Atmos. Environ. 102, 376–383.

Zheng, J., Yamada, M., 2004. Sediment core record of global fallout and Bikini close-in fallout Pu in Sagami Bay, western northwest Pacific margin. Environ. Sci. Technol. 38 (13), 3498–3504.

Zheng, J., Yamada, M., 2006. Plutonium isotopes in settling particles: transport and scavenging of Pu in the western Northwest Pacific. Environ. Sci. Technol. 40 (13), 4103–4108.

Zheng, J., Yamada, M., Wu, F.C., Liao, H., 2009. Characterization of Pu concentration and its isotopic composition in soils of Gansu in northwestern China. J. Environ. Radioact. 100, 71–75.

Zheng, J., Tagami, K., Watanabe, Y., Uchida, S., Aono, T., Ishii, N., Yoshihisa, S., Yoshihisa, K., Fuma, S., Ihara, S., 2012. Isotopic evidence of plutonium release into the environment from the Fukushima DNPP accident. Sci. Rep. 2, 304. https://doi.org/10.1038/srep00304.

Zhu, P., Wu, H., 2018. Origins and transports of the low-salinity coastal water in the southwestern Yellow Sea. Acta Oceanol. Sin. 37 (4), 1–11.